Dynamics of the lower stratospheric circulation response to ENSO

Article

Published Version

www.reading.ac.uk/centaur

Dynamics of the Lower Stratospheric Circulation Response to ENSO

ISLA R. SIMPSON, THEODORE G. SHEPHERD, AND MICHAEL SIGMOND

Department of Physics, University of Toronto, Toronto, Ontario, Canada

ABSTRACT

A robust feature of the observed response to El Niño–Southern Oscillation (ENSO) is an altered circulation in the lower stratosphere. When sea surface temperatures (SSTs) in the tropical Pacific are warmer there is enhanced upwelling and cooling in the tropical lower stratosphere and downwelling and warming in the midlatitudes, while the opposite is true of cooler SSTs. The midlatitude lower stratospheric response to ENSO is larger in the Southern Hemisphere (SH) than in the Northern Hemisphere (NH).

In this study the dynamical version of the Canadian Middle Atmosphere Model (CMAM) is used to simulate 25 realizations of the atmospheric response to the 1982/83 El Niño and the 1973/74 La Niña. This version of CMAM is a comprehensive high-top general circulation model that does not include interactive chemistry. The observed lower stratospheric response to ENSO is well reproduced by the simulations, allowing them to be used to investigate the mechanisms involved. Both the observed and simulated responses maximize in December–March and so this study focuses on understanding the mechanisms involved in that season.

The response in tropical upwelling is predominantly driven by anomalous transient synoptic-scale wave drag in the SH subtropical lower stratosphere, which is also responsible for the compensating SH midlatitude response. This altered wave drag stems from an altered upward flux of wave activity from the troposphere into the lower stratosphere between 20° and 40°S. The altered flux of wave activity can be divided into two distinct components. In the Pacific, the acceleration of the zonal wind in the subtropics from the warmer tropical SSTs results in a region between the midlatitude and subtropical jets where there is an enhanced source of low phase speed eddies. At other longitudes, an equatorward shift of the midlatitude jet from the extratropical tropospheric response to El Niño results in an enhanced source of waves of higher phase speeds in the subtropics. The altered resolved wave drag is only apparent in the SH and the difference between the two hemispheres can be related to the difference in the climatological jet structures in this season and the projection of the wind anomalies associated with ENSO onto those structures.

1. Introduction

El Niño–Southern Oscillation (ENSO) is one of the dominant modes of natural variability in our climate system. The cyclic variation between warm and cold tropical Pacific sea surface temperatures (SSTs) has far-reaching consequences, not just for tropospheric climate but also for the stratosphere.

There are several features of the response to ENSO that are now robust in the observational record and are reproduced in modeling studies. In the troposphere, the direct response to warm ENSO conditions is a warming of the tropical troposphere due to the convective adjustment response to the anomalous SSTs (Chiang and

Corresponding author address: Isla Simpson, Department of Physics, University of Toronto, 60 St George St., Toronto ON M5S 1A7, Canada.
E-mail: isla@atmosp.physics.utoronto.ca

Sobel 2002). ENSO further affects the high latitudes both through zonally asymmetric teleconnection responses (Hoskins and Karoly 1981; Brönnimann 2007, and references therein) and through a zonal mean response (e.g., Robinson 2002; Seager et al. 2003). In the zonal mean picture the warming of the tropical troposphere during El Niño events strengthens the subtropical jets. During NH winter, when the events normally peak, there is an observed equatorward shift of the eddy-driven midlatitude jets and a band of tropospheric cooling in the midlatitudes of both hemispheres (L'Heureux and Thompson 2006), which is attributed to altered upper tropospheric momentum fluxes in response to the strengthened subtropical jet (Robinson 2002; Seager et al. 2003; Lu et al. 2008; Harnik et al. 2010). During La Niña events this zonal mean response switches sign.

In the stratosphere, during NH winter, the polar vortex is warmer and more disturbed during warm ENSO

events (e.g., Sassi et al. 2004; Manzini et al. 2006; Garcia-Herrera et al. 2006; Taguchi and Hartmann 2006). As well as this high-latitude response there is also an altered circulation in the low-latitude lower stratosphere. During warm ENSO conditions there is enhanced upwelling in the tropical lower stratosphere, which is accompanied by cooler temperatures (Reid et al. 1989; Garcia-Herrera et al. 2006; Free and Seidel 2009; Randel et al. 2009) and up to a 15% decrease in ozone for a typical strength El Niño (Randel et al. 2009; Marsh and Garcia 2007; Randel and Thompson 2011). Associated with the compensating downwelling in the extratropics there are midlatitude temperature anomalies that are in phase with ENSO—that is, a warming of the midlatitude lower stratosphere during warm ENSO conditions (Free and Seidel 2009; Randel et al. 2009), with the response being larger in the SH than the NH. The opposite is true of La Niña conditions.

It is the low-latitude stratospheric response to ENSO that is the subject of this study. Although the negative correlation between tropical Pacific SSTs and temperature in the tropical lower stratosphere is a robust feature in the observational record and is reproduced in modeling studies (Hardiman et al. 2007; Calvo et al. 2010), the exact mechanisms by which ENSO influences the circulation of the tropical lower stratosphere remain uncertain.

Garcia-Herrera et al. (2006) speculate that the tropical lower stratospheric temperature response is associated with altered NH planetary wave driving of the large-scale equator-to-pole Brewer–Dobson circulation. On the other hand, a recent study by Calvo et al. (2010), investigating the response in transient simulations with the Whole Atmosphere Community Climate Model (WACCM) GCM, found a dominant role for changes in parameterized orographic gravity wave drag (OGWD) in the NH with a relatively minor contribution from resolved wave drag, particularly for the strongest ENSO events. But neither of these mechanisms can account for the observed midlatitude response in the SH lower stratosphere seen in observations (Free and Seidel 2009). Another mechanism whereby SST anomalies can affect the lower stratosphere is through the convective excitation of quasi-stationary waves (Deckert and Dameris 2008). However, the circulation anomalies associated with these waves are confined to tropical latitudes and are thus unable to explain the observed midlatitude response.

Here, the mechanisms responsible for the tropical upwelling response will be investigated using an ensemble of perturbation runs with a dynamical version of the Canadian Middle Atmosphere Model (CMAM) driven by prescribed SSTs. By using an ensemble of simulations of an extreme El Niño and an extreme La Niña event, the mechanisms involved can be investigated without the complications arising from the additional forcings and long-term changes in a transient climate simulation, and robust statistics can be obtained. In contrast to the above mentioned studies, it is found that transient synoptic-scale resolved wave drag in the SH subtropics dominates the tropical upwelling response, which also explains the observed SH midlatitude response. However, a contribution from OGWD in the NH is also present, in agreement with Calvo et al. (2010).

The transient resolved wave drag response to ENSO is further confirmed using transient simulations with the coupled chemistry version of CMAM that are forced with observed SSTs from 1960 to 2000. This allows for a comparison with simulations forced with all different types and strengths of ENSO events, including coupled chemistry and with a different horizontal resolution, to test the robustness of our results.

The structure of the paper is as follows. In section 2 the model simulations are described. Section 3 discusses the response to SST anomalies in the perturbation runs. It is demonstrated that resolved wave drag in the SH subtropics plays a dominant role in the lower stratospheric circulation anomaly. Section 4 then confirms the presence of this wave drag anomaly in transient simulations of the twenty-first century with the chemistry CMAM. Section 5 then returns to the perturbation experiments for a more detailed analysis of the cause of the resolved wave drag change, and finally discussions and conclusions are presented in section 6.

2. The model experiments

To investigate the mechanisms responsible for the response to ENSO in the low-latitude lower stratosphere, perturbation experiments with the dynamical version of CMAM (Scinocca et al. 2008) are used. This is a comprehensive atmospheric general circulation model with T63 horizontal resolution and 71 levels in the vertical stretching from the surface to 0.0006 hPa (~100 km).

The perturbation experiments are performed by first running a control simulation of 30-yr length, taking the first 5 yr as spinup. This control simulation has monthly varying SSTs specified at the lower boundary according to the 1960–2000 climatology of the observed SSTs from the Hadley Centre Global Sea Ice and Sea Surface Temperature (HadISST1) dataset (Rayner et al. 2003). The El Niño and La Niña simulations consist of an ensemble of 25 members starting from the beginning of September of each year of the control run simulation.

Thus, each member differs in its atmospheric initial conditions. Each ensemble member is run for a year with perturbed SSTs given by the monthly varying climatological SSTs plus a monthly varying El Niño or La Niña anomaly. The SST anomalies are only applied between 50°N and 50°S and there is a slight ramping up of the SST anomalies to the observed values over the first half of September. For El Niño, SSTs from September 1982 to September 1983 are used, whereas for La Niña SSTs from September 1973 to September 1974 are used: these represent two of the largest ENSO events of the latter half of the twentieth century. The SST anomalies are obtained from the HadISST dataset by subtracting the seasonally varying climatology for the 1960–2000 period.

The monthly mean SST anomalies for each of the simulations together with the average anomaly over the Niño-3.4 region are shown in Fig. 1. Here we shall only be concerned with the season when the lower stratospheric temperature response is largest, which is during NH winter, when the SST anomalies peak. Therefore, only the SST anomalies from September to April are shown in Fig. 1 and there will be a focus on the response in the months from December to March (DJFM). Although there is a slight difference in the timing of the peak SST anomalies between the El Niño and La Niña events, both these events have SST anomalies of at least 1 K in the Niño-3.4 region for the whole of the December–March period.

For the comparison with transient simulations of the twentieth century, data from the chemistry version of the CMAM will be used. This is very similar to the dynamical CMAM but includes interactive chemistry and has a lower horizontal resolution (T31). An ensemble of three simulations was performed for the second Chemistry Climate Model Validation activity (CCMVal-2; Eyring et al. 2010). These simulations were forced with time-varying greenhouse gases, volcanic aerosols, and solar irradiance according to the CCMVal-2 REFB1 specifications (Morgenstern et al. 2010). Of importance for this study is that the simulations were transient runs forced with observed SSTs for the 1960–2000 period from the HadISST1 dataset and therefore contain all different types and strengths of ENSO events.

3. Results of the SST perturbation experiments

Figure 2 shows the response in zonal mean temperature $\overline{T}$ and zonal wind $\overline{u}$ for the El Niño and La Niña perturbation runs, both averaged over the period December–March. Here, and throughout the paper, the quoted significance levels are calculated using a Student's t test, taking each ensemble member as an independent realization.

For El Niño there is a strong warming in the tropical troposphere associated with the convective adjustment response to the anomalous SSTs (Chiang and Sobel 2002), which through thermal wind balance acts to strengthen the zonal wind in the subtropics. While there is heating in the troposphere throughout the whole tropics there is a zonally asymmetric component to the heating as well (not shown), which consists of the dumbbell-shaped warming that straddles the equator in the Pacific associated with the off-equatorial anticyclonic circulations set up by the altered tropical convection (Yulaeva and Wallace 1994). The enhanced zonal wind in the subtropics is therefore also localized to the Pacific region in each hemisphere, as will be discussed further in section 5.

The observed zonal mean extratropical response consisting of an equatorward shift of the eddy-driven jet and a band of oppositely signed temperature anomalies in the midlatitude troposphere is evident. There is an asymmetry in this midlatitude response between the NH and SH with the response being weaker and more merged with the subtropical response in the NH. This midlatitude response also has an important zonally asymmetric component, which will also be discussed further in section 5. As mentioned previously, several studies have examined the mechanisms responsible for the zonal mean tropospheric midlatitude response (e.g., Robinson 2002; Seager et al. 2003; Lu et al. 2008; Harnik et al. 2010). While there is agreement that this response is associated with altered upper tropospheric momentum fluxes, the exact mechanism is still under discussion. For the purpose of this study, which focuses on the stratospheric response, the tropospheric temperature and zonal wind response will be taken as given and the mechanism behind it not discussed further.

In the stratosphere there is a notable asymmetry in the NH high-latitude response between El Niño and La Niña, with El Niño resulting in a warmer polar stratosphere and a weaker polar vortex but no significant response for the La Niña case. This is in agreement with Manzini et al. (2006) and Sassi et al. (2004) and implies that the high-latitude response must be associated with a different mechanism than the lower-latitude response, which is evident for both El Niño and La Niña. As this study focuses on the lower-latitude response, the NH polar response to El Niño will not be discussed further.

In the stratosphere there is a clear out-of-phase temperature response in the tropics with cooling (warming) for El Niño (La Niña) along with an oppositely signed temperature response in the extratropics. Note that the extratropical temperature anomaly is larger in the SH than in the NH, which is consistent with the observations in that season (Free and Seidel 2009; Randel et al. 2009).
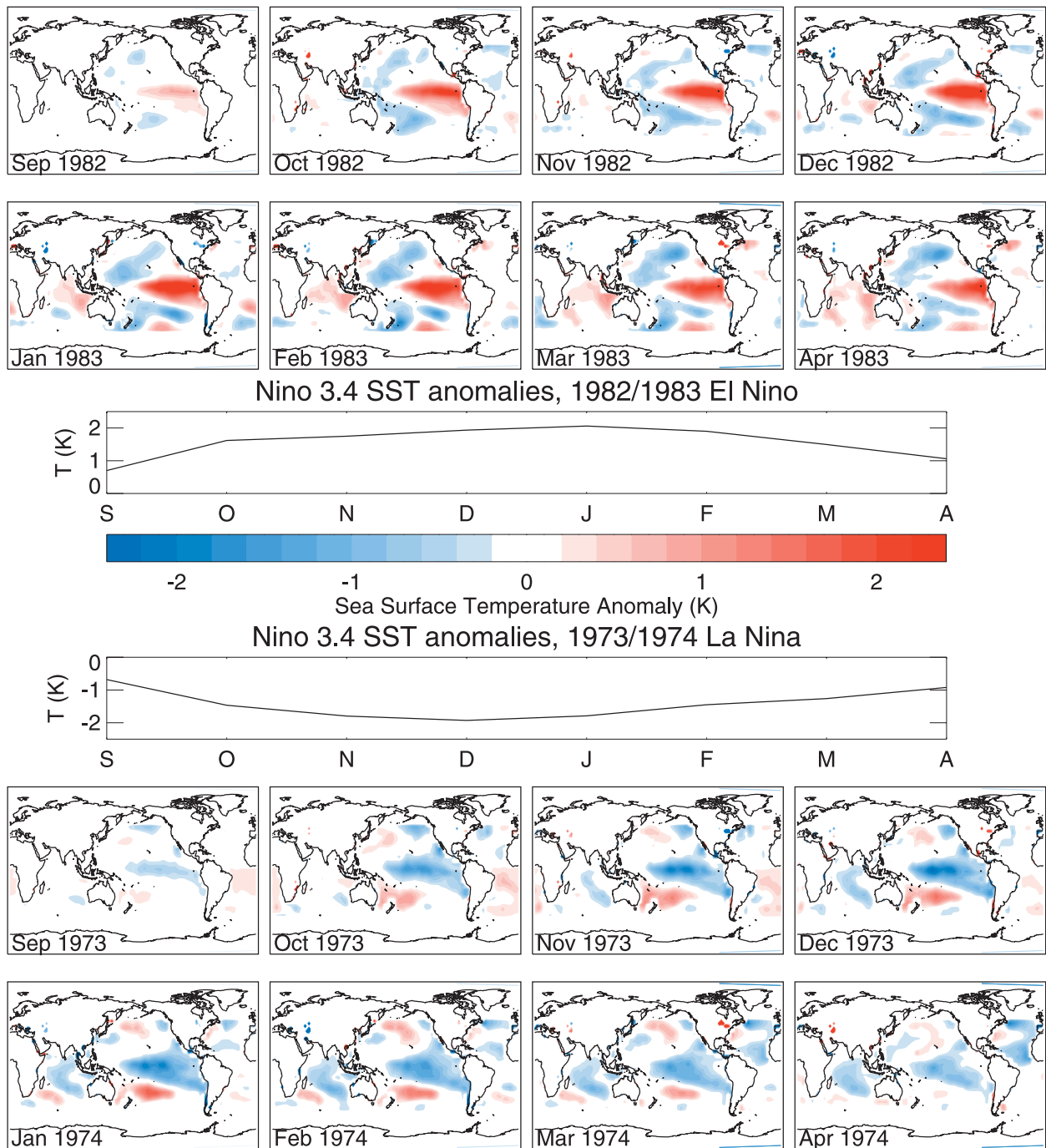
FIG. 1. SST anomalies that are added to monthly varying climatological SSTs, along with the average anomaly over the Niño-3.4 region, for (top) the El Niño and (bottom) the La Niña simulations. Months from September until April are shown.

At the lowest stratospheric levels [∼(130–77) hPa] there is a strong zonally asymmetric component (not shown) that resembles the dumbbell-shaped anomaly in the troposphere but is of opposite sign, which is also consistent with observations (Yulaeva and Wallace 1994). At higher levels, the dumbbell shape is no longer

apparent and there is cooling in the whole of the tropical lower stratosphere in response to El Niño, suggesting a wave-driven upwelling.

It seems clear that (with the exception of the NH high-latitude response) the overall response is rather symmetric between El Niño and La Niña (i.e., the responses
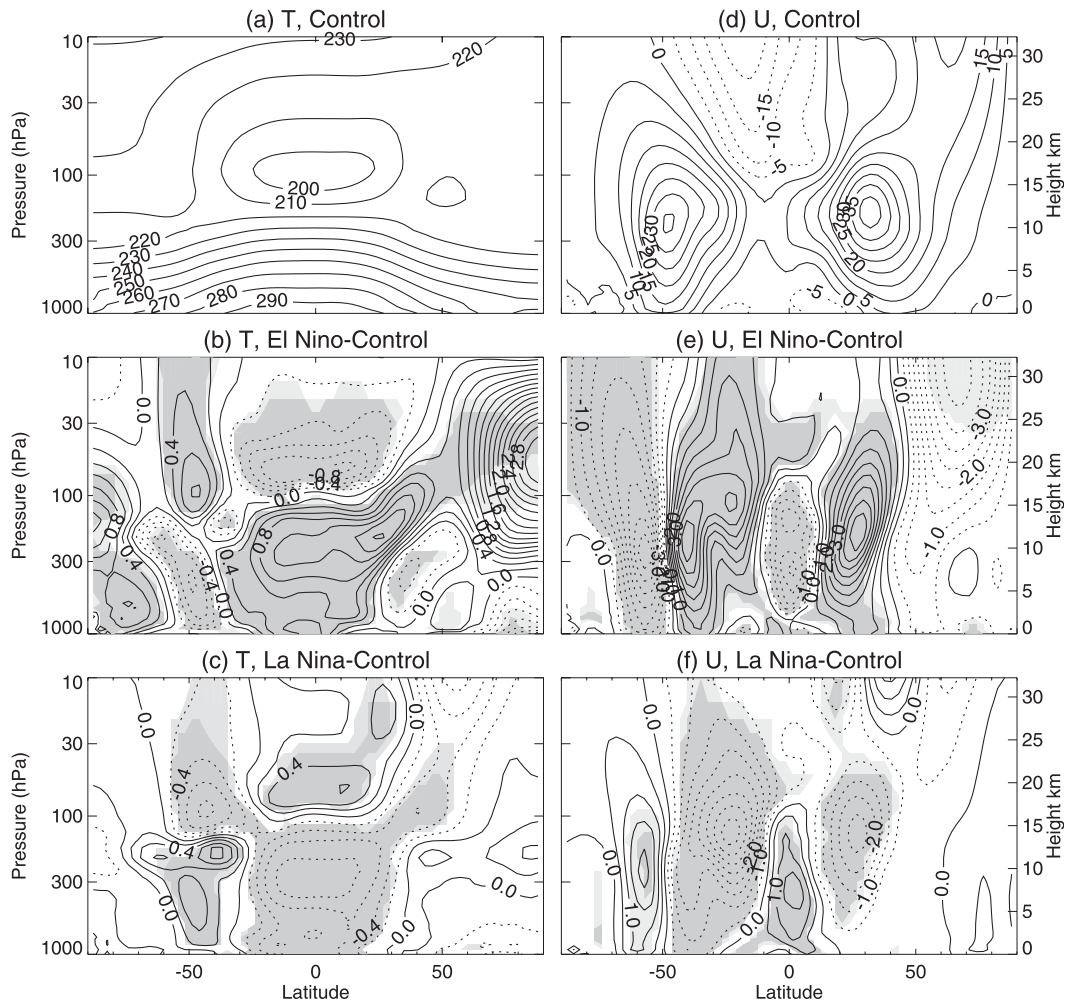
FIG. 2. (a)–(c) Zonal mean temperature and (d)–(f) zonal mean zonal wind averaged over DJFM for (top) control, (middle) El Niño-control, and (bottom) La Niña-control. Contour intervals (CIs) are: temperature, control = 10 K and anomalies = 0.2 K; zonal wind, control = 5 m s^{-1} and anomalies = 0.5 m s^{-1}. Light and dark gray regions are where the anomalies are significantly different from zero at the 95% and 99% levels, respectively. Dotted contours indicate negative values.

are similar but of opposite sign). There is some difference in the magnitudes, which may be associated with the fact that the La Niña SST anomalies peak slightly later in the season or that part of the response is somehow related to the NH high-latitude response, which is absent for La Niña. But overall the response is similar and the aspects to be discussed in the following are rather symmetric between El Niño and La Niña. Therefore, for succinctness the results will now be presented as the difference between El Niño and La Niña rather than the difference of each individually from the control.

Figure 3 examines the residual vertical velocity $\overline{w}^*$ response in the lower stratosphere for DJFM. In the La Niña averaged vertical velocity (Fig. 3a) (which for these purposes of comparing El Niño with La Niña may

be considered the "climatology") there is upwelling in the tropics and downwelling in the extratropics associated with the large-scale equator-to-pole Brewer–Dobson circulation. This circulation is strongest in the winter hemisphere, due to the strong resolved wave drag there, and thus the downwelling is strongest at NH high latitudes in this season.

Figure 3b then shows the difference in $\overline{w}^*$ between El Niño and La Niña, which demonstrates a significant increase in tropical upwelling for El Niño, maximizing in the lower stratosphere. Figure 3b suggests that the $\overline{w}^*$ response may be regarded as consisting of two circulation cells. The dominant cell consists of (for El Niño but vice versa for La Niña) increased upwelling in the lowermost stratosphere in the SH tropics and increased
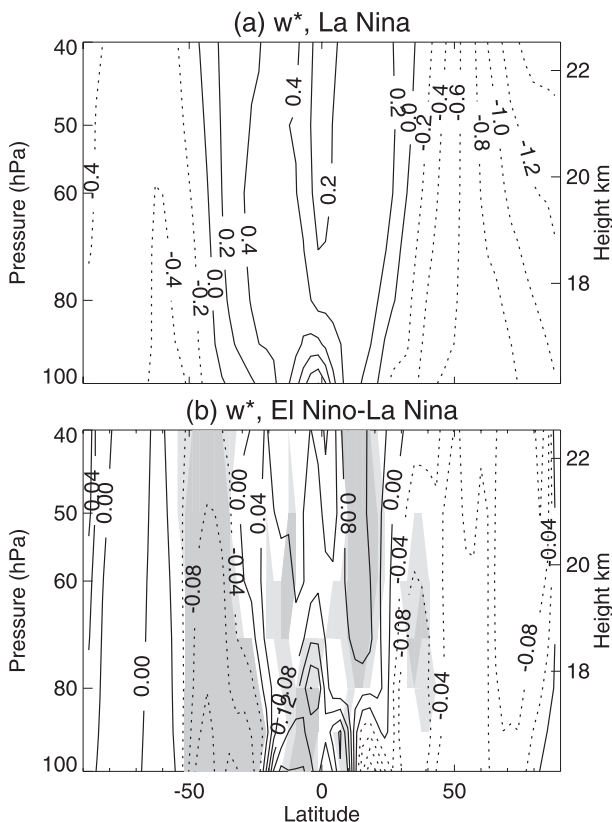
FIG. 3. DJFM zonal mean residual vertical velocity $\overline{w}^*$ for (a) the La Niña simulations (CI = 0.2 mm s^{-1}) and (b) the difference between El Niño and La Niña (CI = 0.02 mm s^{-1}). Positive values denote upwelling and light and dark gray regions are significantly different from zero at the 95% and 99% levels, respectively. Dotted contours indicate negative values.

downwelling in the SH extratropics. There also appears to be a secondary circulation cell located slightly higher up and in the NH that consists of increased upwelling between around 10° and 20°N, above around 70 hPa, and increased downwelling in the NH extratropics. The meridional flow associated with these circulation changes crosses angular momentum contours in the tropics (not shown), implying that they are driven by changes in wave drag. The reason for distinguishing between these two circulation anomalies will become apparent in the following as the wave drag anomalies responsible for each are examined. There are three sources of wave drag in the stratosphere in these simulations: resolved wave drag, parameterized OGWD, and parameterized non-OGWD. There are no significant anomalies in non-OGWD (not shown). The resolved wave drag is related to the Eliassen–Palm (E–P) flux divergence ($\nabla \cdot \mathbf{F}$) by $\nabla \cdot \mathbf{F}/\rho a \cos\phi$ where the E–P flux components are defined following Andrews et al. (1987, p. 128) as

$$\mathbf{F}_\phi = \rho_o a \cos\phi\left(\overline{u}_z \frac{\overline{v'\theta'}}{\overline{\theta}_z} - \overline{u'v'}\right),$$

$$\mathbf{F}_z = \rho_o a \cos\phi\left(\hat{f}\frac{\overline{v'\theta'}}{\overline{\theta}_z} - \overline{w'u'}\right). \quad (1)$$

Figure 4 shows that during El Niño there is an enhanced convergence (i.e., more negative divergence) of resolved wave activity flux in the SH subtropics with only small anomalies occurring in the NH. This feature is clearly the origin of the enhanced SH midlatitude downwelling. Furthermore, this resolved wave drag anomaly is dominated by transient synoptic-scale waves. This is demonstrated by the decomposition into the contribution from zonal wavenumbers 1 to 3 (Fig. 4d) and zonal wavenumbers greater than 3 (Fig. 4c). The resolved wave drag anomaly in the SH subtropical lower stratosphere is therefore not associated with the excitation of quasi-stationary waves associated with altered convection or with altered large-scale planetary wave forcing. Figure 4b shows the change in OGWD. Here the dominant anomalies are in the NH centered around 30°N, where the climatological OGWD is a maximum associated with the Tibetan plateau.

These two wave drag anomalies account for the two circulation patterns mentioned previously in the discussion of Fig. 3. In particular, the OGWD anomaly is the primary cause of the anomalous upwelling in the NH tropics and downwelling in the NH extratropics, while the resolved wave drag anomaly is the primary cause of the anomalous tropical upwelling in the lowermost stratosphere that occurs shifted slightly into the SH and the downwelling in the SH extratropics.

Which type of wave drag dominates the tropical upwelling response can be determined using the procedure of Holton (1990). This procedure makes use of the downward control principle (Haynes et al. 1991), which states that the residual circulation streamfunction $\overline{\psi}$ at a particular level is related to the integral of the forcing $\overline{F}$ (m s^{-2}) above that level according to

$$\overline{\psi}_{DC}(\phi, p) = \frac{\cos\phi}{g}\int_p^0 \frac{\overline{F}(\phi, p')}{\hat{f}}dp', \quad (2)$$

where $\hat{f} = f - (a\cos\phi)^{-1}\partial(\overline{u}\cos\phi)/\partial\phi$ and f is the Coriolis parameter. The residual vertical velocity $\overline{w}^*$ is related to the streamfunction by

$$\overline{w}^*_{DC} = \frac{gH}{pa\cos\phi}\frac{\partial\overline{\psi}_{DC}}{\partial\phi}, \quad (3)$$

where H is the scale height, taken to be 7 km. Although the downward control principle does not apply locally within the deep tropics, following the procedure of
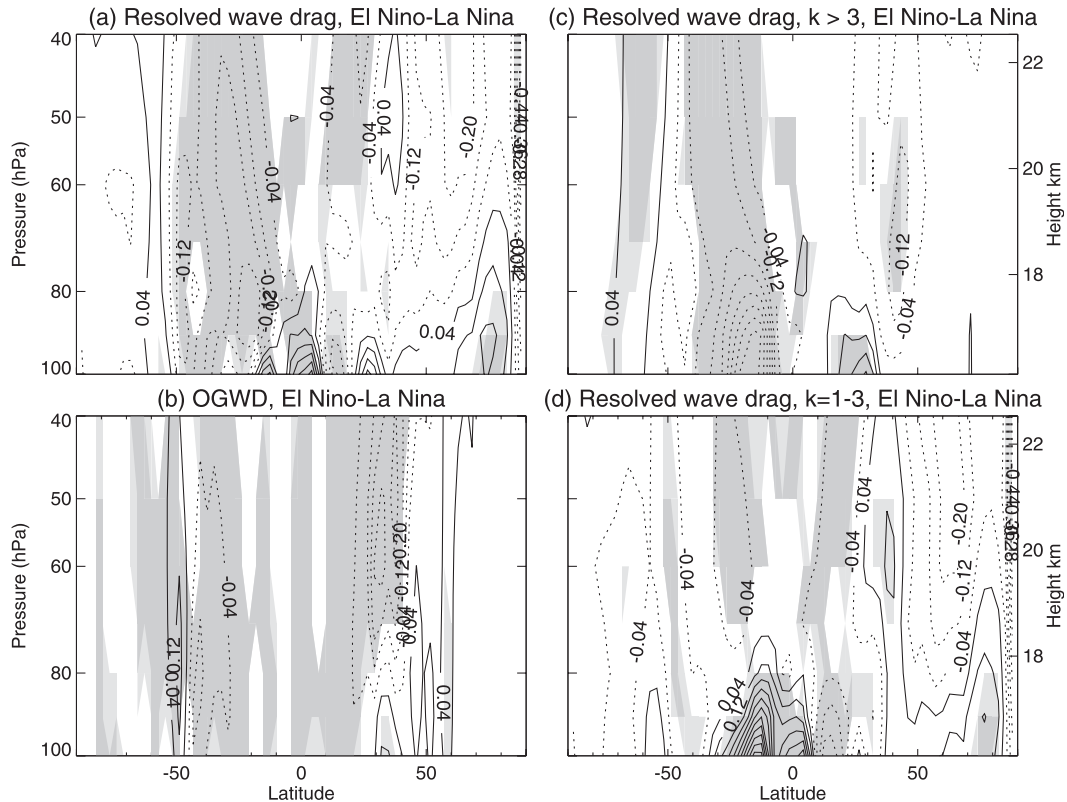
FIG. 4. DJFM wave drag anomalies for El Niño minus La Niña: (a) resolved wave drag, (b) orographic gravity wave drag, (c) resolved wave drag associated with zonal wavenumbers > 3, and (d) resolved wave drag associated with wavenumbers 1–3. All contour intervals are 0.06 m s^{-1} day^{-1} (note the CIs are staggered about 0). Light and dark gray regions are statistically significant at the 95% and 99% levels, respectively, and dotted contours indicate negative values of divergence (i.e., an enhanced convergence of wave activity).

Holton (1990) it can be used to determine the wave driving anomaly responsible for the tropical average vertical velocity anomaly $\langle \overline{w}^* \rangle$ between latitude bounds $-\phi_o$ and $+\phi_o$ according to

$$\langle \overline{w}^*_{\mathrm{DC}} \rangle (p) = \frac{\int_{-\phi_o}^{\phi_o} \overline{w}^*_{\mathrm{DC}}(\phi, p) a \cos\phi \, d\phi}{\int_{-\phi_o}^{\phi_o} a \cos\phi \, d\phi}, \qquad (4)$$

provided that $\overline{f}$ is nonzero at those latitudes. Using (2) and (3), this amounts to

$$\langle \overline{w}^*_{\mathrm{DC}} \rangle (p) = \frac{\dfrac{gH}{p} \left| \dfrac{\cos\phi}{g} \int_p^0 \dfrac{\overline{F}(\phi, p')}{\hat{f}} \, dp \right|_{-\phi_o}^{\phi_o}}{\int_{-\phi_o}^{\phi_o} a \cos\phi \, d\phi}; \qquad (5)$$

that is, the downward control integral is evaluated at the latitude bounds that define the tropical region, and the difference taken. This is equivalent to calculating the tropical upwelling that balances the mean extratropical downwelling.

Figure 5 shows the results of this downward control integral within the latitude bounds $\pm 23°$. This latitude bound is chosen following Calvo et al. (2010), who performed a similar analysis looking at the tropical lower stratospheric upwelling response to ENSO in the WACCM GCM. It is considered to be far enough equatorward that the source of the tropical upwelling is captured while being far enough poleward that the downward control integral is valid. The total $\langle \overline{w}^*_{\mathrm{DC}} \rangle$ (dotted line) can be compared with the model $\langle \overline{w}^* \rangle$ (solid line). Complete agreement is not expected because of transience and nonlinearity but, given that the agreement is reasonably close, this method provides a convenient way of estimating the relative importance of the different forcings to the circulation.

Decomposing the vertical velocity response into contributions from resolved wave drag, OGWD, and non-OGWD it is clear that the resolved wave drag by far dominates the tropical upwelling response, with OGWD only contributing around one-fifth of the response. This result differs from that of Calvo et al. (2010) since, although they found that the resolved wave drag in the SH
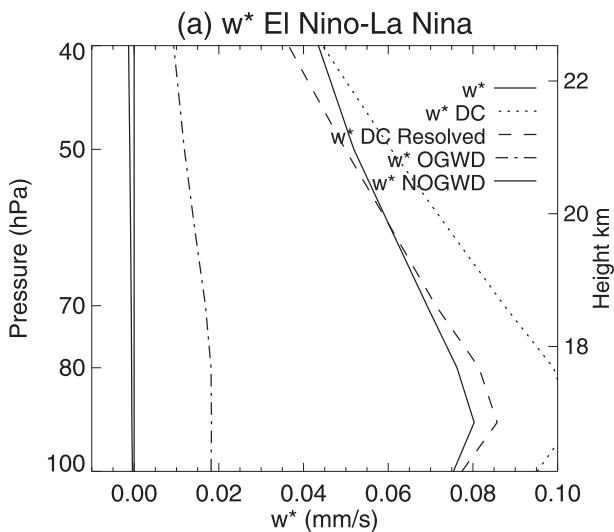
FIG. 5. Downward control contributions to the mean tropical upwelling difference between El Niño and La Niña in DJFM. The latitude bounds of the calculation are 23°N and 23°S.

subtropics and the OGWD both play a role, they found that in the strongest ENSO events the OGWD dominates in the response. The mechanism they proposed for the OGWD anomaly is the same as that for the OGWD response to climate change: a strengthening of the upper flank of the subtropical jet in the NH shifts the breaking levels of orographic gravity waves up into the lower stratosphere (Li et al. 2008; McLandress and Shepherd 2009). It should be noted that the OGWD anomaly lies right on the edge of the subtropics. Therefore, if the latitude bounds for the integral were shifted poleward, there would be more of a role for OGWD in the mean tropical upwelling [cf. Fig. 21 of McLandress and Shepherd (2009)], whereas if they were shifted equatorward the resolved wave drag would completely dominate. The extent to which OGWD plays a role in the mean tropical upwelling may therefore be very sensitive to the latitudinal distribution of the parameterized OGWD, which depends on the jet and the details of the OGWD parameterization. This is a likely cause of the difference between this result and that of Calvo et al. (2010). On the other hand, the broad latitudinal extent of the resolved wave drag anomaly means that its extent of influence is much less sensitive to the latitudinal bounds of the downward control integral. That it is a robust feature of the response to ENSO can also be seen in Fig. 3 of Calvo et al. (2010), although they did not go into the details of the mechanism behind this feature. Importantly, the resolved wave drag anomaly also provides an explanation of the midlatitude warming in the SH lower stratosphere found in both these model simulations and in the observations, which is larger and more significant

than the NH midlatitude response (Free and Seidel 2009).

To summarize the results of this section, warm ENSO conditions are associated with enhanced upwelling in the tropical lower stratosphere and downwelling in the mid-latitude lower stratosphere. The residual circulation anomalies cross angular momentum contours and therefore are driven by wave drag anomalies. This anomalous circulation consists of a SH component primarily driven by transient synoptic-scale resolved wave drag and a NH component primarily driven by OGWD. This circulation response induces a cooling in the tropical lower stratosphere and warming in the extratropics with the SH response being stronger than the NH response, consistent with observations. Since the resolved wave drag anomaly is predominantly due to zonal wavenumbers 4 and greater, it is associated with altered synoptic-scale eddy fluxes rather than wave fluxes associated with anticyclonic circulations set up in the tropical Pacific in response to ENSO, which are of larger scale.

4. Comparison with the twentieth-century chemistry CMAM simulations

The lower stratospheric response to ENSO in the perturbation runs will now be compared to the response in transient simulations from 1960 to 2000 with the interactive chemistry version of CMAM.[1] This allows an examination of the response to all different types and strengths of ENSO events as well as a comparison with the response in a different (and lower resolution) version of the model, to test the robustness of our results.

To separate the ENSO signal from other natural and anthropogenic forcings that are specified in this version of the model, the monthly mean data were first regressed onto a linear trend, monthly global mean aerosol optical depth (Sato et al. 1993) and monthly varying total solar irradiance (obtained online from http://www.geo.fu-berlin.de/en/met/ag/strat/forschung/SOLARIS/Input_data/index.html) and then each of these contributions was removed. Composites were then taken of the DJFM average for El Niño and La Niña periods. These were defined, following Trenberth (1997), to be times when the magnitude of the SST anomalies in the Niño-3.4 region exceeded 0.4 K for 6 months or more. This criterion gives 14 El Niños and 11 La Niñas in the 1960–2000 period (listed in Table 1) and since there are three ensemble members, this gives a composite difference between 42 El Niños and 33 La Niñas.

---

[1] Note that there is no QBO in these simulations.

TABLE 1. List of El Niño and La Niña DJFM seasons used for the ENSO composites of the chemistry CMAM simulations (e.g., 63/64 indicates the season from December 1963 to March 1964). The SST values listed are the DJFM mean Niño-3.4 SST anomalies from climatology (K).

El Niño		La Niña	
Year	SST	Year	SST
63/64	0.46	64/65	−0.55
65/66	1.00	70/71	−1.26
68/69	0.74	71/72	−0.49
69/70	0.44	73/74	−1.66
72/73	1.26	74/75	−0.54
76/77	0.57	75/76	−1.26
77/78	0.51	84/85	−0.99
79/80	0.40	88/89	−1.54
82/83	2.06	95/96	−0.55
86/87	1.05	98/99	−1.19
87/88	0.60	99/00	−1.43
91/92	1.42		
94/95	0.84		
97/98	2.00		

The results are shown in Fig. 6. A very similar temperature pattern to the response in Figs. 2b and 2c can be seen in Fig. 6a, namely an out-of-phase temperature anomaly in the tropical lower stratosphere and an oppositely signed temperature anomaly in the midlatitude lower stratosphere. It is also quite clear that the warming around 45° latitude in the lower stratosphere is much larger in the SH than in the NH. Figure 6b also shows very similar anomalies in the vertical velocity as Fig. 3b with the same two distinct circulation patterns. In the NH there is, as before, anomalous upwelling between around 5° and 10°N above about 70 hPa and downwelling in midlatitudes, which is driven by the OGWD (Fig. 6d). This is again as discussed in Calvo et al. (2010). But, as before, the strongest circulation response occurs below 70 hPa and consists of upwelling shifted slightly to the south of the equator and downwelling in southern midlatitudes, and is driven by resolved wave drag in the SH subtropics (Fig. 6c).

In this lower-resolution version of CMAM both the climatological OGWD and the OGWD anomalies extend farther equatorward. The result is that the OGWD becomes relatively more important for the tropical average upwelling, in line with the results of Calvo et al. (2010). This again suggests that, when integrated across the tropics, the exact partitioning of the wave drag can be very sensitive to resolution and OGWD parameterization. Nevertheless, the results in Fig. 6c still show a dominant role for transient resolved wave drag in the SH subtropics. Therefore, we now return to the perturbation experiments for a more detailed examination of the mechanism behind this anomaly.

5. Investigation into the mechanism behind the resolved wave drag response to ENSO

a. The SH resolved wave drag response

There are several possibilities for the cause of the resolved wave drag response in the SH. A change in the position of the Rossby wave critical layers, either meridionally or vertically, could act to shift the location of synoptic-scale wave breaking, thereby changing the E–P flux convergence in the lower stratosphere. Alternatively there could be a change in the source of the waves from the lower troposphere, or some alteration of the propagation properties of the atmosphere such that more wave activity is able to propagate into the subtropical lower stratosphere.

We begin by examining the first of these possibilities: a shift in critical line position. The zonal wind anomalies for the El Niño and La Niña perturbation runs in Figs. 2e and 2f demonstrate that the thermal wind response to altered latitudinal temperature gradients arising from the tropical SST perturbations strengthens the wind in the subtropics for El Niño compared to La Niña. Rossby waves break in the vicinity of the critical line where the zonal wind equals the phase speed (Randel and Held 1991). When they break, there is a convergence of E–P flux. It follows that this change in the zonal wind can change where the waves break, shifting the region of breaking latitudinally or vertically and thereby altering the E–P flux convergence in the subtropical lower stratosphere. Indeed, a meridional shift in the critical lines has been invoked to explain the midlatitude tropospheric response to ENSO (Robinson 2002; Lu et al. 2008), and a vertical shift has recently been proposed by Shepherd and McLandress (2011) as the mechanism behind the contribution of resolved waves to the strengthened Brewer–Dobson circulation that models predict in response to climate change.

In the following, eddy cospectra will be used to investigate whether a change in the position of the critical lines is responsible for the altered wave drag in the subtropical lower stratosphere. Following the method of Hayashi (1971), the eddy fluxes of heat $\overline{v'T}$ and momentum $\overline{u'v'}$ can be decomposed into contributions from different wavenumbers and frequencies at each latitude. From this, Randel and Held (1991) demonstrated that the E–P flux components and their divergence can be determined as a function of latitude and phase speed, allowing the spatial distribution of wave drag to be related to critical line location. The cospectra are shown as a function of angular phase speed c_A, which is related to regular phase speed c by $c_A = c/\cos\phi$. Angular phase speed is used as it is conserved following propagation in the meridional plane and thus meridional E–P flux anomalies at upper
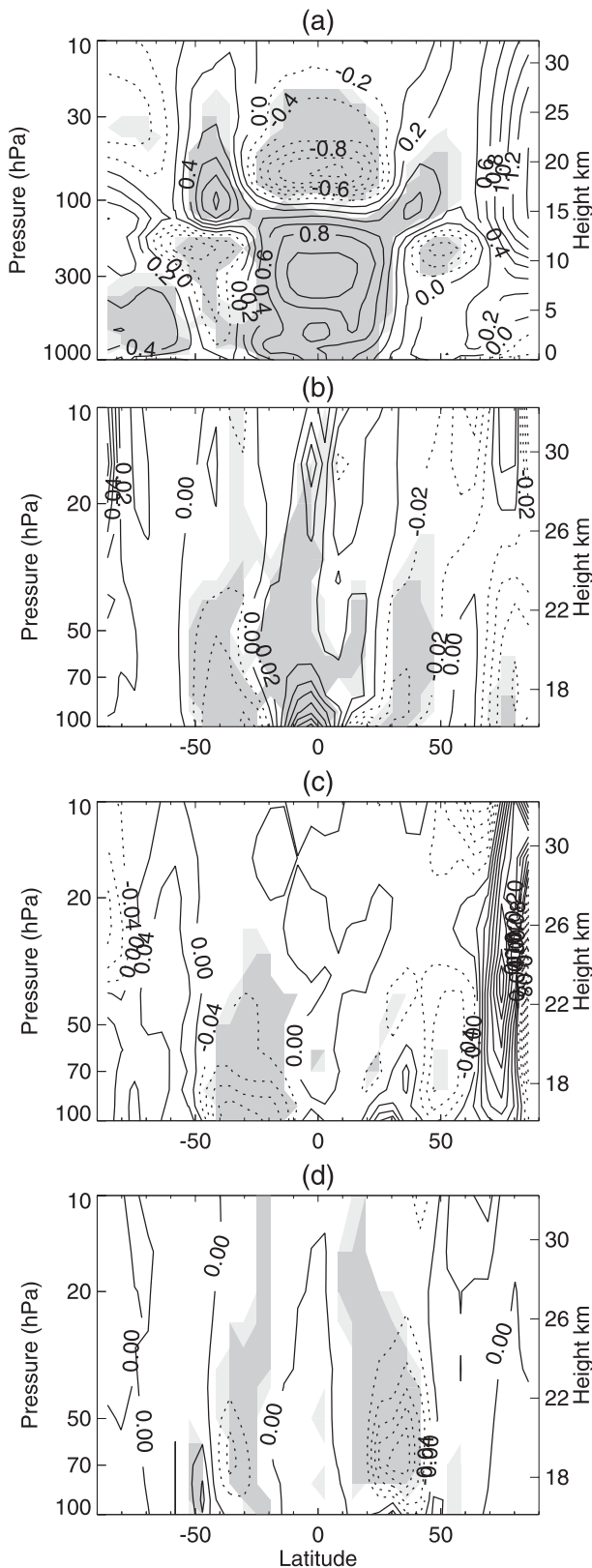
FIG. 6. Difference between El Niño and La Niña composites of the chemistry CMAM 1960–2000 simulations in DJFM. (a) Zonal mean

levels can be related to altered vertical E–P flux at lower levels (Randel and Held 1991). When using angular phase speed the critical line is given by $\bar{u}/\cos\phi$.

The results for the SH are shown in Fig. 7, which shows the quasigeostrophic vertical E–P flux $\mathbf{F}_z$ at the 211-hPa level, meridional E–P flux $\mathbf{F}_\phi$ at the 64-hPa level, and resolved wave drag $(\nabla \cdot \mathbf{F}/\rho a \cos\phi)$ at the 64-hPa level. For the wave drag and $\mathbf{F}_\phi$ component, 64 hPa is chosen because it is located in the region where the wave drag anomalies are strong. For $\mathbf{F}_z$, 211 hPa is used to examine the change in upward propagation of wave activity from the troposphere into the stratosphere.

In the La Niña climatology there is an upward flux of wave activity from the troposphere to the stratosphere that is rather well restricted to the latitudes within the low- and high-latitude critical lines (Fig. 7a). The maximum in upward E–P flux occurs at progressively lower latitudes for lower (angular) phase speeds. This wave activity propagates upward and equatorward as indicated by the meridional E–P flux (Fig. 7c), until the waves break, resulting in the maximum convergence slightly poleward of the low-latitude critical line (Fig. 7e). The wave drag maximum is not completely restricted by the critical line, with some convergence occurring on the equatorward side of it.

If a meridional shift in critical line position were important, then one would expect the wave drag anomaly to have a dipolar structure and to be enveloped by the control and anomaly critical lines. In Fig. 7f this is not the case. Rather, Fig. 7b indicates that the increased convergence of wave activity during El Niño at 64 hPa in the subtropics is related to an enhanced upward flux of wave activity across the 211-hPa level, predominantly between 20° and 40°S and at lower latitudes for lower phase speeds. This wave activity then propagates upward and equatorward ($\mathbf{F}_\phi$ in Fig. 7d), resulting in E–P flux convergence anomalies for El Niño compared to La Niña (Fig. 7f). It should be noted that all aspects of the cospectrum analysis discussed above are symmetric (but of opposite sign) between the El Niño and La Niña differences from the control, permitting further confidence in their robustness.

This change in upward propagation between around 20° and 40°S at 211 hPa is also not associated with a critical line shift at that level. In this sense ENSO

←

temperature (CI = 0.2 K), (b) residual vertical velocity (CI = 0.02 mm s^{-1}), (c) transient resolved wave drag (CI = 0.04 m s^{-1} day^{-1}), and (d) OGWD (CI = 0.04 m s^{-1} day^{-1}). Note the different vertical scale in (a). Light and dark gray shading indicates regions that are statistically significant at the 95% and 99% confidence levels, respectively.
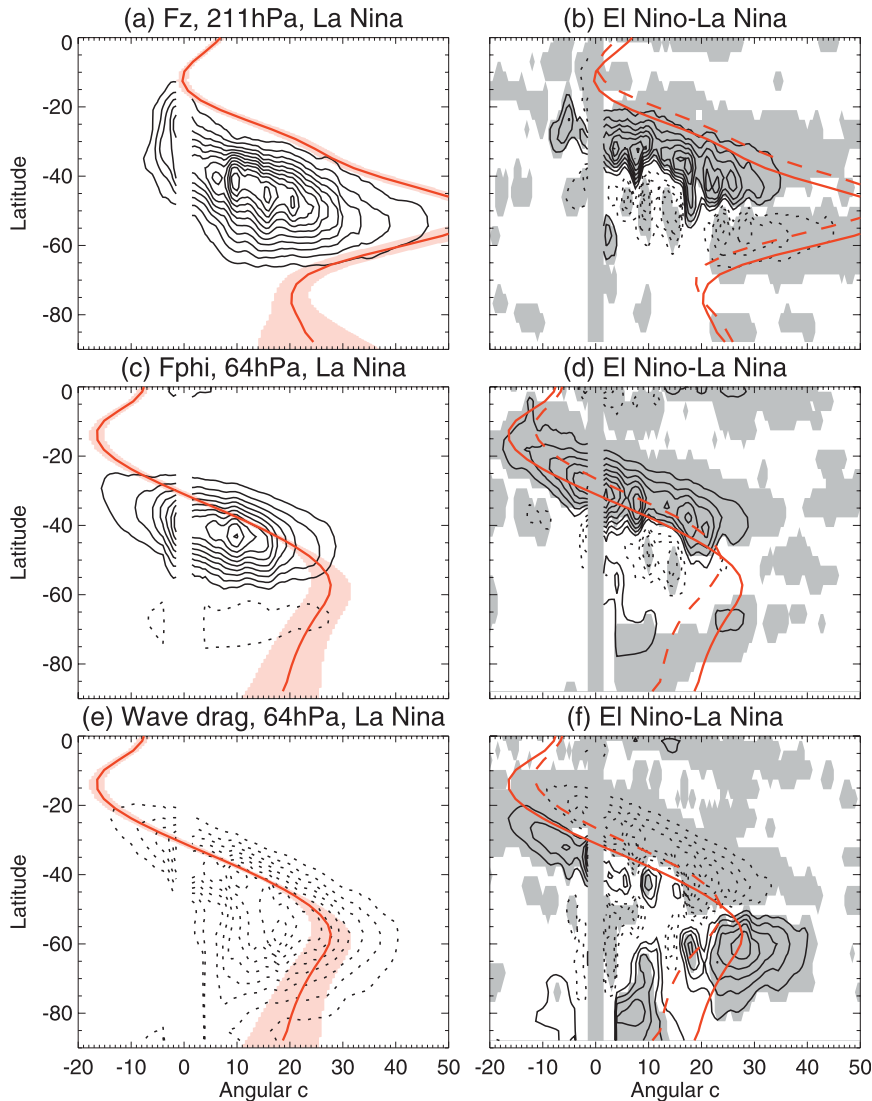
FIG. 7. Cospectra of (top) vertical E–P flux on the 211-hPa level, (middle) meridional E–P flux on the 64-hPa level, and (bottom) wave drag ($\mathbf{V} \cdot \mathbf{F}/\rho a \cos\phi$) on the 64-hPa level. (left) The La Niña climatology and (right) the difference between El Niño and La Niña for the DJFM season. Contour intervals are as follows: (a) 1×10^3 kg s^{-2} Δc^{-1}, (b) 5×10^2 kg s^{-2} Δc^{-1}, (c) 1×10^4 m^3 s^{-2} Δc^{-1}, (d) 5×10^3 m^3 s^{-2} Δc^{-1}, (e) 5×10^{-3} m s^{-1} day^{-1} Δc^{-1}, and (f) 2.5×10^{-3} m s^{-1} day^{-1} Δc^{-1}, where Δc is 0.5 m s^{-1}. The solid red line shows the La Niña $\bar{u}/\cos\phi$ and the dashed line shows the El Niño $\bar{u}/\cos\phi$. For the La Niña climatology plots, the red shading indicates ± 1 standard deviation about the mean in $\bar{u}/\cos\phi$. For the difference plots, gray regions are statistically significant at the 95% level. Dotted contours indicate negative values.

differs significantly from climate change where a much larger shift in the critical line position in the lower stratosphere is produced, and the wave drag anomalies are clearly associated with waves that could not previously propagate into that region (Shepherd and McLandress 2011).

The conclusion from this initial cospectrum analysis is that a shift in the position of the critical line in the lower stratosphere, either meridionally or vertically, does not appear to play a significant role in the lower stratospheric resolved wave drag anomaly. Rather, the anomaly appears to be related to an increased flux of wave activity from the troposphere into the stratosphere between 20° and 40°S for El Niño compared to La Niña. This can be further seen in Fig. 8, which shows the latitude–pressure cross section of the total transient E–P flux anomalies
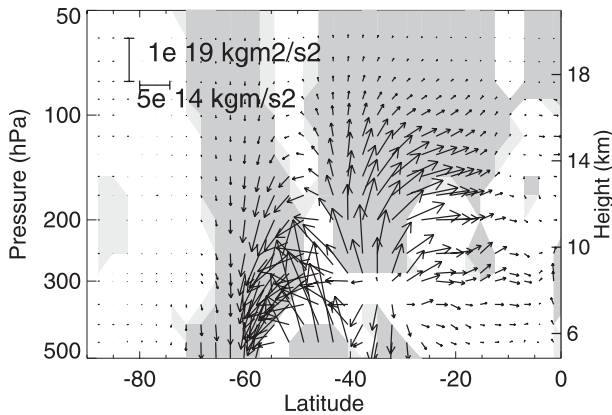
FIG. 8. El Niño–La Niña transient E–P flux vector anomalies during DJFM scaled as in Dunkerton et al. (1981). Light and dark gray regions are where the vertical E–P flux component anomaly is significantly different from zero at the 95% and 99% levels, respectively.

between 500 and 50 hPa for El Niño/La Niña. This is calculated by subtracting the stationary component from the total E–P flux, where the stationary component is calculated from monthly mean anomalies from the zonal mean, and the E–P flux vectors $\mathbf{F}_\phi$ and $\mathbf{F}_z$ have been scaled following Dunkerton et al. (1981). It is clear that there is an increase in the upward flux of wave activity into the lower stratosphere centered around 20°–40°S for El Niño compared to La Niña. At first inspection this appears to be unrelated to enhanced upward flux of wave activity coming from below. However, a more detailed analysis of the cospectra and the variations with longitude reveals otherwise.

Figure 9 presents the longitudinal variations of the zonal wind response to ENSO on the 283-hPa level (i.e., in the upper troposphere). This reveals a considerable zonal asymmetry in the zonal wind response in the SH: the accelerated wind in the subtropics is localized to the Pacific region, whereas the equatorward shifted eddy-driven midlatitude jet occurs at all longitudes other than the Pacific region. Thus, if the altered flux of eddy activity into the lower stratosphere is in response to this altered zonal wind structure, then it is reasonable to expect that the response may differ between these regions, given that they are of large zonal extent (i.e., larger than the typical scale of transient eddies).

In the following the cospectra and changes in eddy fluxes will be examined in two longitude regions: one covering Pacific longitudes where there is an accelerated wind in the subtropics, denoted Pacific, and the other at longitudes other than the Pacific where there is an equatorward shift of the eddy-driven midlatitude jet, denoted Not Pacific. This gives considerably more insight into the origins of the $\mathbf{F}_z$ anomalies than the zonal mean analysis
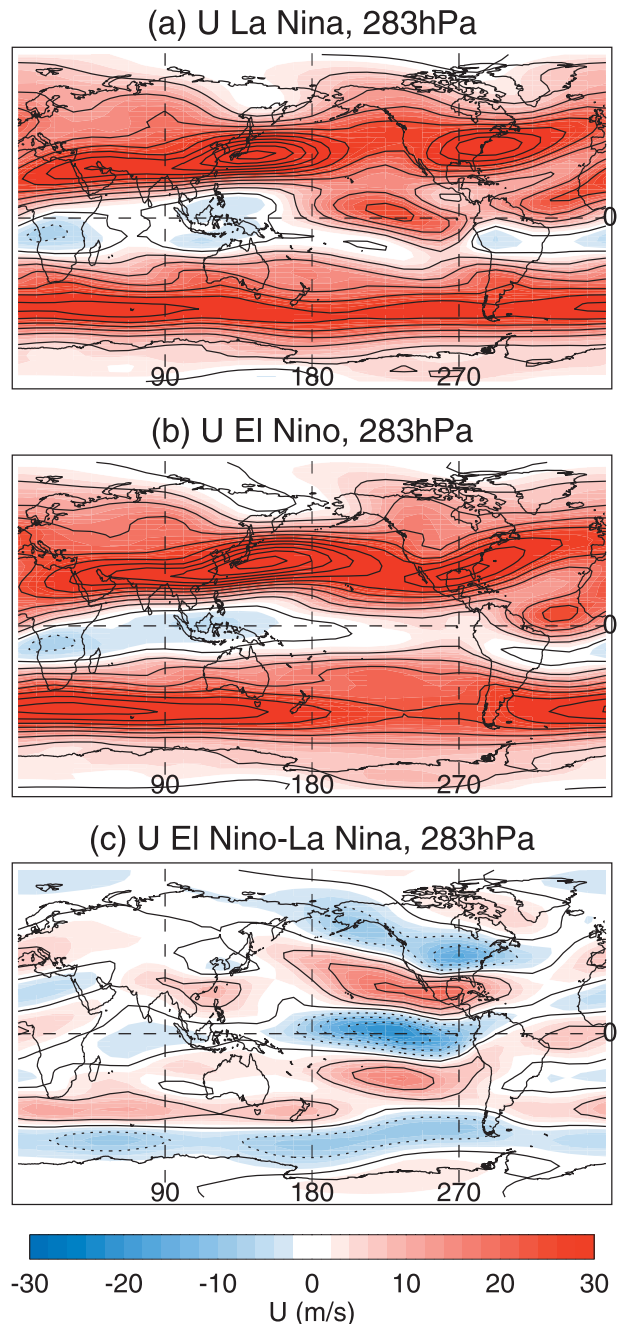

FIG. 9. Zonal mean zonal wind on the 283-hPa level for (a) the DJFM climatology for La Niña, (b) the DJFM climatology for El Niño, and (c) the difference between El Niño and La Niña. Lined contours are drawn at 6 m s^{-1} intervals and dotted contours indicate negative values.

does. When calculating the cospectra over localized longitude regions, the fields of interest are tapered using the taper functions shown in the top row of Fig. 10 before the Fourier transform is applied. These taper functions show the longitudes included in each region. In the calculation

of the E–P fluxes the cospectra of $\overline{u'v'}$ and $\overline{v'T'}$ are used where here an overline represents the average over the longitude sector. However, the zonal wind and potential temperature of the basic state that also appear in the E–P flux formulas are that of the full zonal mean, no matter which longitude sector is considered. This is done so that any difference in E–P fluxes between regions is related only to the eddy fluxes rather than to the basic state used. In this way the contribution to the zonal mean E–P flux anomalies can be decomposed into the contributions from the eddy fluxes in the different longitude sectors.

The 211-hPa $\mathbf{F}_z$ La Niña climatology and the El Niño − La Niña difference for each region are shown in the second and third rows, respectively, of Fig. 10. The contributions from Pacific and Not Pacific can be seen to approximately add up to the total, suggesting that the dominant changes are captured by the sum of these two regions. From the anomalies it becomes quite apparent that the upward $\mathbf{F}_z$ across that level consists of two components of distinct origin: the high phase speed anomalies ($c_A \sim$ 12–30 m s^{-1}) occur in Not Pacific, whereas the low phase speed anomalies ($c_A \sim$ 5–15 m s^{-1}) occur in Pacific.

Examination of the cospectra at 902 hPa (rows 4 and 5 of Fig. 10) reveals that each of these anomalies in vertical E–P flux can be related to an anomalous source of eddies from the lower troposphere. While it may be somewhat simplistic to divide the eddy fluxes in this way since, for example, $\mathbf{F}_z$ anomalies in the upper troposphere in Pacific will contain a component that is due to eddies that develop at lower levels upstream in Not Pacific and vice versa, it seems clear that the distinct eddy flux anomalies at 211 hPa can be related to anomalies in the lower troposphere within that same region. Moreover, a rough calculation of the ratio of vertical to zonal group velocities using the Q–G dispersion relation for vertically propagating Rossby waves in a stratified atmosphere suggests that for typical synoptic-scale eddies, a wave packet would travel on the order 10°–30° of longitude in the time it would take for the vertical propagation between the two levels, which is much smaller than the width of the longitude regions considered. So, it seems reasonable to consider that a large proportion of the wave activity crossing the 211-hPa level in either longitude region originated in that same longitude region.

A first thing to note from the climatological $\mathbf{F}_z$ cospectra that is important in the interpretation of the results is that different factors appear to be important in determining the maximum $\mathbf{F}_z$ at different phase speeds. For higher phase speeds ($c_A >$ 10 m s^{-1}) the maximum in $\mathbf{F}_z$ occurs at the latitude of the jet (i.e., in the region of maximum baroclinicity), as expected. At lower phase speeds, however, this is not the case. Rather, there are two wings of maximum $\mathbf{F}_z$ on the flanks of the jet rather than in the region of maximum baroclinicity, suggesting that other factors are important for the growth of the low phase speed eddies.

Turning now to the anomalies in Not Pacific, the dominant feature at low levels is a meridional dipole in $\mathbf{F}_z$, predominantly for the higher phase speeds. This meridional dipole follows the equatorward shift of the region of maximum baroclinicity and extends throughout the troposphere (see Fig. 12f). A fraction of the enhanced wave activity on the equatorward side of the jet continues to propagate up into the lower stratosphere, giving the E–P flux convergence anomalies seen at high phase speeds in Fig. 7f.

The lower phase speed anomalies in Pacific are not so straightforward to interpret. They are also likely to be more important in the lowest-latitude tropical upwelling since these low phase speed eddies can propagate deeper into the tropics. The anomalous $\mathbf{F}_z$ on the 902-hPa level in Pacific (Fig. 10, middle of row 5) consists of several components. First, at high phase speeds there is a reduction in $\mathbf{F}_z$ centered around 55°–60°S, which can be related to the strong deceleration in zonal wind at those latitudes and consequent reduction in baroclinicity. But there are also significant anomalies at lower phase speeds. There is an enhanced $\mathbf{F}_z$ between $\sim$(40°–70°S) at 902 hPa. These eddies mostly break on the poleward side of the jet and lower than 211 hPa, which is why they are not visible in the 211-hPa plot. But of importance for the stratospheric wave drag anomaly is the enhancement at lower latitudes [$\sim$(20°–35°S)]. These anomalies can be related to the enhanced $\mathbf{F}_z$ at 211 hPa that propagates up into the lower stratosphere, resulting in the low phase speed component of Fig. 7f.

So, what is causing this important change in the production of low phase speed eddies? Some insight can be gained from the studies of Lee (1997) and Kim and Lee (2004). They revealed the presence of eddies, which they refer to as interjet disturbances (IJDs), that grow in the region between the midlatitude and subtropical jets. In both observations and idealized GCMs these studies have found that, aside from the typical growth of eddies that occurs along the midlatitude jet center where baroclinicity is a maximum, there are disturbances that grow in the region between the subtropical and midlatitude jets, and these disturbances have a lower phase speed. The exact nature of these IJDs is not yet known. Kim and Lee (2004) note that they may be associated with the barotropic governor mechanism (James and Gray 1986; James 1987), which relates the ability of eddies to grow to the barotropic shear. The interjet region, being a region of weak barotropic shear, represents a location where the eddies are more likely to grow.
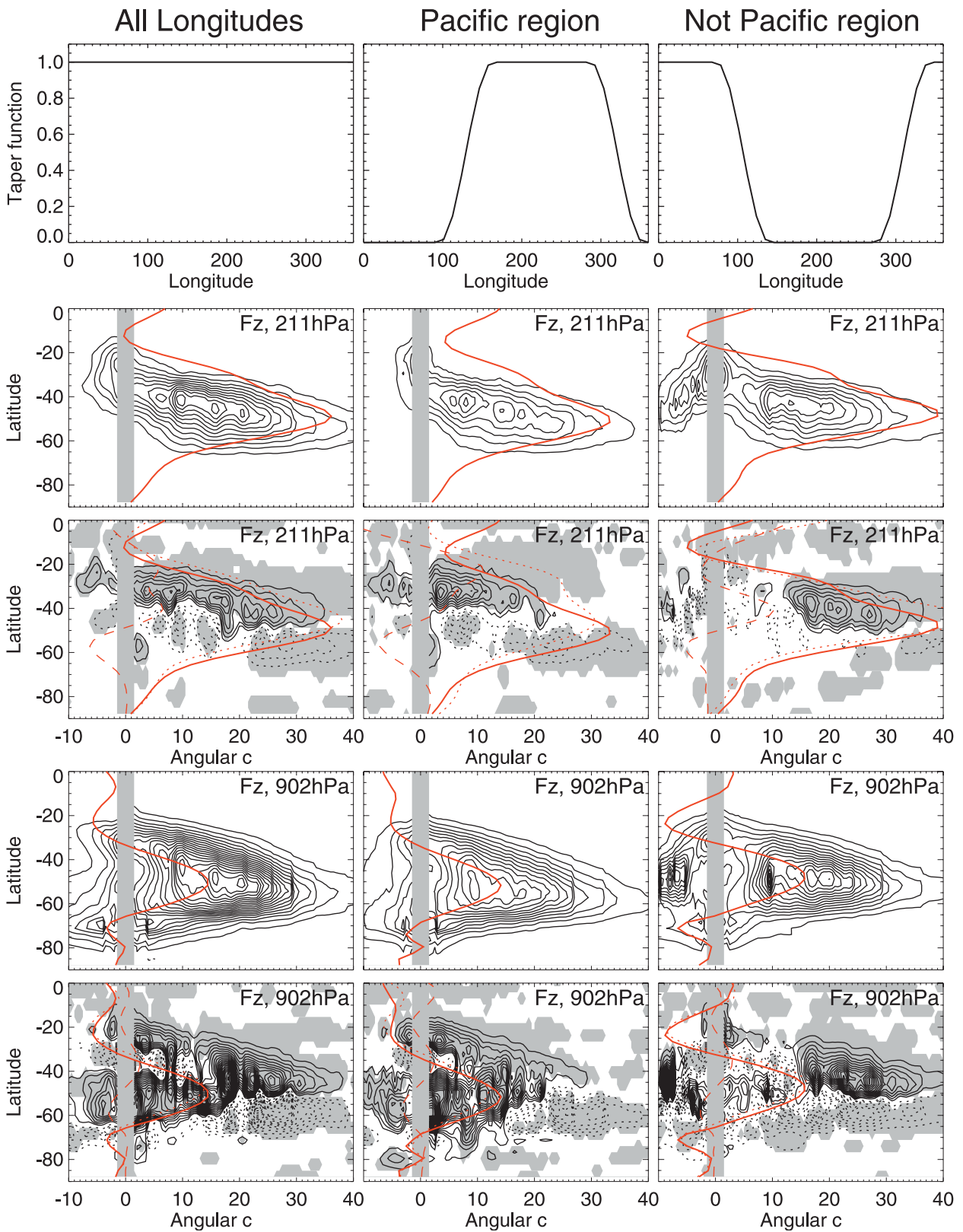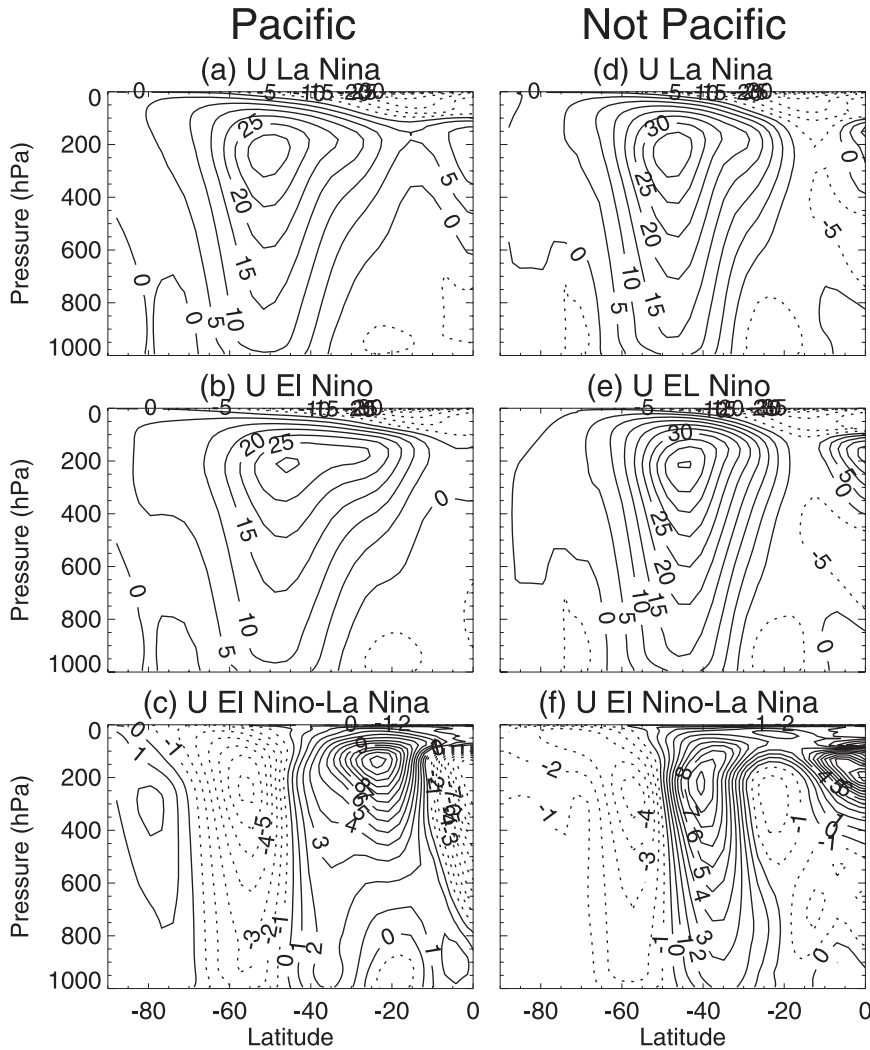
FIG. 11. DJFM zonal mean zonal wind averaged over (a)–(c) the longitudes in Pacific where no tapering is applied and (d)–(f) the longitudes in Not Pacific where no tapering is applied, for (top) La Niña, (middle) El Niño, and (bottom) El Niño − La Niña. Dotted contours indicate negative values.

The change in the production of low phase speed eddies in response to ENSO may be related to this mechanism. Comparison of Figs. 11a and 11b demonstrates that in Pacific the accelerated wind in the subtropics results in a much more prominent distinction between the midlatitude and subtropical jets, which is then consistent with

an enhancement of these low phase speed disturbances in the interjet region. However, an important point to note is that the E–P fluxes associated with these disturbances are not visible throughout the whole troposphere. Rather, they maximize at the surface and then again at the tropopause in both the climatology and the anomalies, and

←

FIG. 10. (row 1) The taper functions used for the calculation of cospectra over the zonal mean, Pacific, and Not Pacific regions. (row 2) The La Niña climatological vertical E–P flux cospectra on the 211-hPa level, CI = 1×10^3 kg s^{-2} Δc^{-1}, and the red line shows the La Niña climatology $\overline{u}/\cos\phi$ at that level averaged over the longitudes where no tapering is applied. (row 3) As in row 2, but for the El Niño − La Niña difference; the solid, dotted, and dashed red lines show the La Niña, El Niño, and El Niño − La Niña $\overline{u}/\cos\phi$ at that level averaged over the longitudes where no tapering is applied. (row 4) As in row 2, but for the vertical E–P flux on the 902-hPa level, a contour interval of 2×10^3 kg s^{-2} Δc^{-1} is used. (row 5) As in row 3, but for the 902-hPa level. All plots show the DJFM season, and $\Delta c = 0.5$ m s^{-1}.
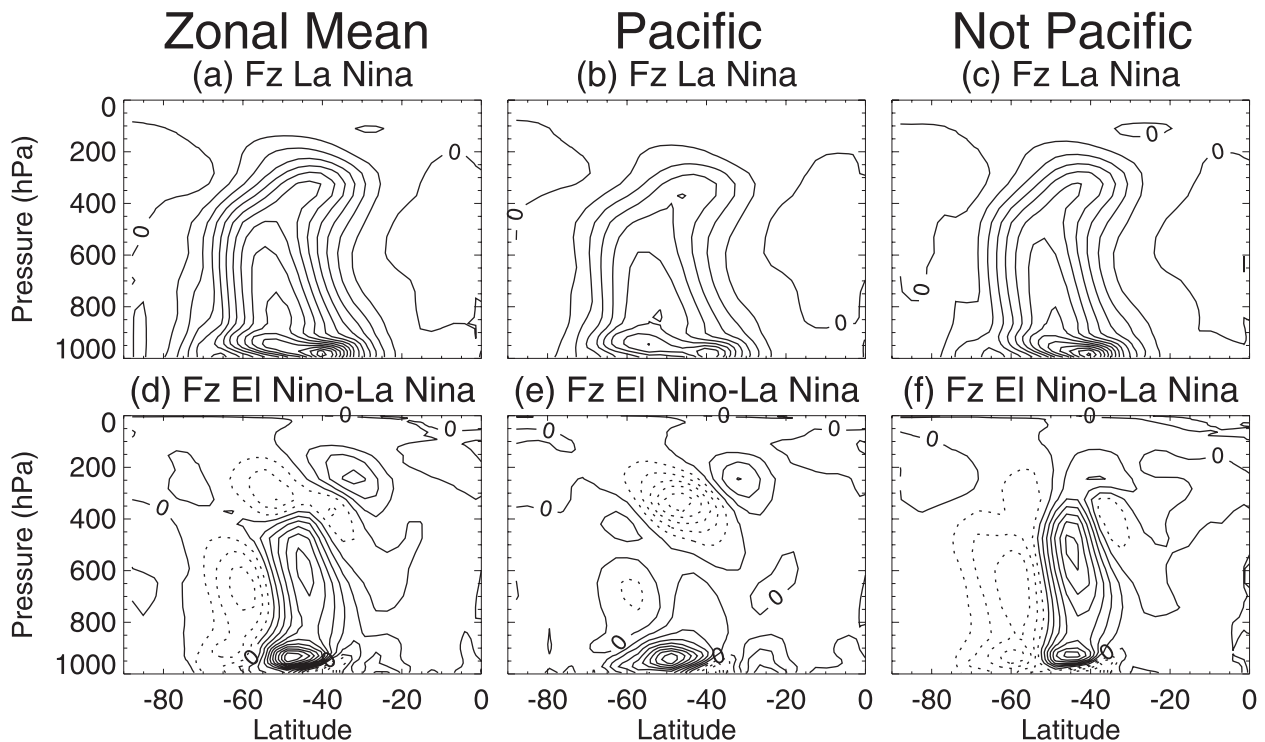
FIG. 12. (a)–(c) Climatological $\mathbf{F}_z$ summed over all phase speeds and (d)–(f) difference in the climatological $\mathbf{F}_z$ between El Niño and La Niña for (left) the zonal mean, (middle) Pacific, and (right) Not Pacific. All plots are averages over the DJFM season.

are not readily apparent in between (see Figs. 12b,e), so they could easily be missed by examination of, for example, $\mathbf{F}_z$ at 700 hPa. This may be different from the low phase speed waves in the more idealized GCM experiments of Kim and Lee (2004), which are visible at 700 hPa. The reason for this is a subject that requires further investigation but is beyond the scope of this study.

To summarize this analysis of the SH eddy fluxes, the enhanced convergence in the subtropical lower stratosphere seen in Fig. 7f consists of two components of distinct origin. There is a high phase speed component originating from the Not Pacific region, where there is an equatorward shift of the eddy-driven midlatitude jet, and a lower phase speed component originating in the Pacific region, where the accelerated wind in the subtropics results in a region of weak barotropic shear in the interjet region and an enhancement of the low phase speed disturbances there. We now ask whether the explanation for the altered resolved wave drag in the SH is consistent with the absence of a resolved wave drag anomaly in the NH.

b. The NH response

The longitudinal variations in the zonal wind response on the 283-hPa level in the NH can also be seen

in Fig. 9. This NH zonal wind response and the mechanisms behind it have been discussed in detail by Harnik et al. (2010). The first thing to note is that the equatorward shift of the midlatitude jet outside the Pacific sector is not evident in the NH. Much like in the SH, there is an enhanced zonal wind in the subtropics of the NH Pacific region. However, unlike in the SH, this enhanced zonal wind does not increase the separation between the subtropical and midlatitude jets. In fact, quite the opposite occurs because of the climatological state in the NH in that season. Figures 9a and 13a show that for the La Niña climatology, a low-latitude jet exists over the equator together with a midlatitude zonal wind maximum that sits at a slightly lower latitude than in the SH. The easterly anomaly over the equator in response to El Niño removes the equatorial jet, while the subtropical wind increase actually occurs in the interjet region (Figs. 13b,c). As a result, the superposition of the zonal wind anomalies in the NH Pacific onto the zonal wind climatology reduces the presence of the interjet region and enhances the barotropic shear on the equatorward side of the jet. This difference between the NH and SH Pacific wind response can be seen clearly by comparison of Figs. 11 and 13.
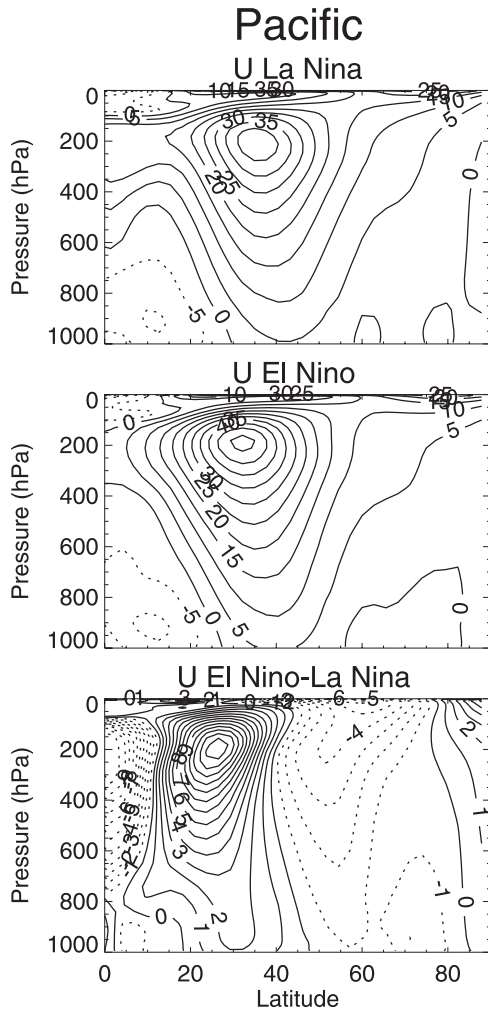
Pacific

FIG. 13. DJFM zonal wind averaged over the Pacific region (150° to 290° longitude) for the NH for (top) La Niña, (middle) El Niño, and (bottom) El Niño − La Niña.

The wave drag cospectra on the 64-hPa level in Figs. 14a and 14b demonstrate that in the NH there is an increase in E–P flux convergence in response to El Niño, but only at high phase speeds. At low phase speeds there is actually a decrease and so in total there is very little wave drag anomaly in the NH midlatitudes (as seen in Fig. 4). The vertical E–P flux anomalies on the 902-hPa level (Fig. 14d) suggest that the lower stratospheric wave drag anomalies are related to a change in the source of eddies from below, with an enhancement at high phase speeds and a reduction at low phase speeds. The cospectra over the Pacific and Not Pacific regions show that most of this $\mathbf{F}_z$ anomaly occurs in the Pacific sector (not shown). The high phase speed anomaly is likely associated with the equatorward shift of the midlatitude jet in the Pacific sector, much like the equatorward shift in Not Pacific in the SH. But, in the NH the projection of the subtropical

zonal wind anomaly in the Pacific region onto the climatology does not have the same effect as in the SH and there is actually a decrease in the low phase speed eddies such that, in total, there is only a very small increase in wave drag in the NH.

6. Discussion and conclusions

The mechanisms responsible for the observed low-latitude circulation response in the lower stratosphere to ENSO during the December–March season have been investigated using SST perturbation experiments with the dynamical version of CMAM. We focus on this season since both the SST anomalies and the lower stratospheric circulation response maximize then. There are two contributors to this circulation response: OGWD in the NH subtropics, as discussed in Calvo et al. (2010), and transient synoptic-scale-resolved wave drag in the SH subtropics. In the perturbation experiments it is found that the resolved wave drag anomaly dominates the tropical average upwelling and that the midlatitude downwelling anomaly is much stronger in the SH than the NH, which is consistent with the observed lower stratospheric temperature anomalies (Free and Seidel 2009). Very similar wave drag anomalies are also found in transient simulations of the twentieth century with a lower-resolution version of the chemistry CMAM, suggesting that both the SH resolved wave drag anomaly and the NH OGWD anomaly are robust responses to ENSO, although their relative contribution to the mean tropical upwelling is somewhat sensitive to model specification.

The mechanism behind the OGWD response to ENSO can be understood via the same mechanism proposed for the OGWD response to climate change: a strengthening of the subtropical jet in the NH shifts the location of gravity wave breaking upward (Li et al. 2008; McLandress and Shepherd 2009; Calvo et al. 2010). However, the analogy between ENSO and climate change cannot be drawn for the resolved wave drag response as quite different mechanisms appear to operate in the two situations, even though they both lead to enhanced tropical upwelling that maximizes in northern winter. For one thing, the resolved wave drag response to climate change includes a significant contribution in the NH subtropics that is not apparent in the ENSO response. Furthermore, Shepherd and McLandress (2011) demonstrate the importance of a critical line shift in the predicted stratospheric resolved wave drag response to climate change, but the cospectrum analysis here suggests that such a mechanism is not relevant to the ENSO response.

Instead, the enhanced convergence of wave activity in the SH subtropical lower stratosphere for El Niño
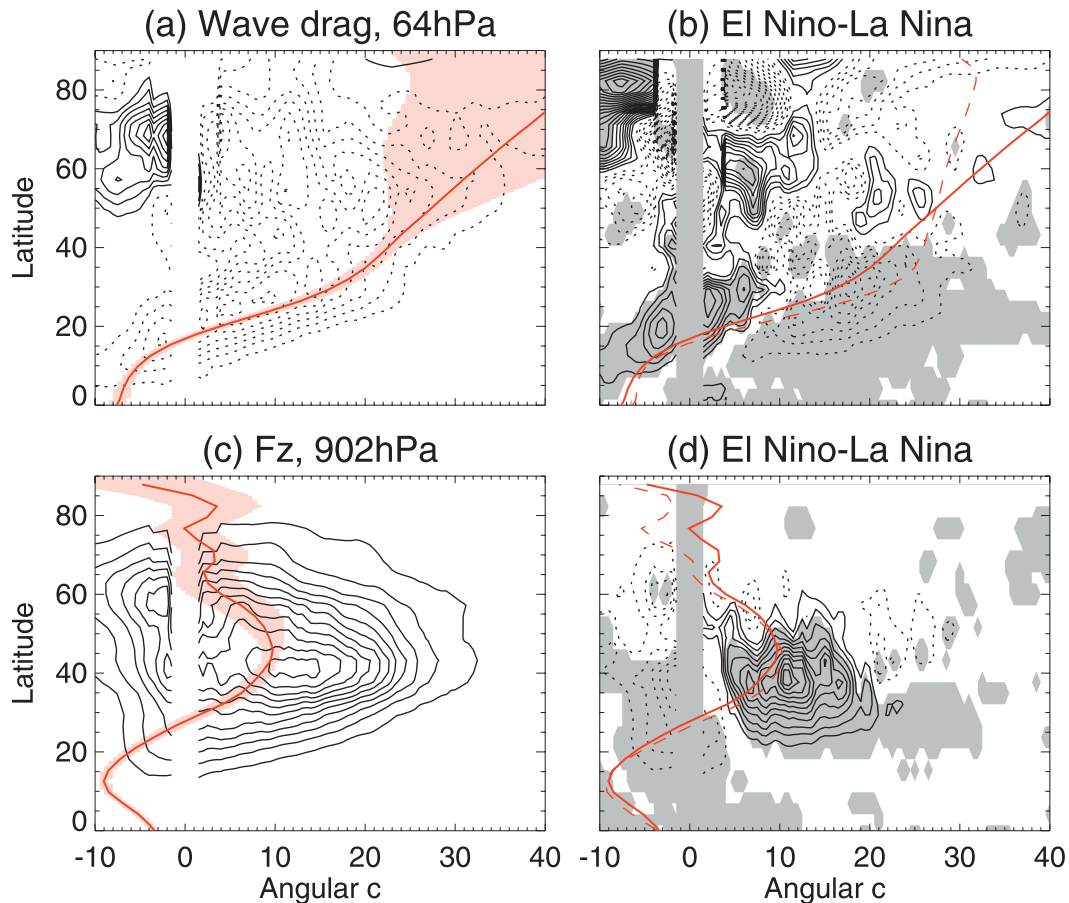
FIG. 14. DJFM cospectra for the NH (a) La Niña wave drag on the 64-hPa level (CI $= 5 \times 10^{-3}$ m s^{-1} day^{-1} Δc^{-1}), (b) wave drag on the 64-hPa level for the difference between El Niño and La Niña (CI $= 2.5 \times 10^{-3}$ m s^{-1} day^{-1} Δc^{-1}), (c) La Niña vertical E–P flux on the 902-hPa level (CI $= 5 \times 10^{3}$ kg s^{-2} Δc^{-1}), and (d) El Niño − La Niña difference in vertical E–P flux on the 902-hPa level (CI $= 2 \times 10^{3}$ kg s^{-2} Δc^{-1}). Here, $\Delta c = 0.5$ m s^{-1}. The solid red lines in all plots show the La Niña $\overline{u}/\cos\phi$ at that level. The red shading in (a) and (c) indicates ± 1 standard deviation about the mean in $\overline{u}/\cos\phi$, and the dashed red lines in (b) and (d) show the El Niño $\overline{u}/\cos\phi$ at that level.

compared to La Niña arises from an increase in the upward propagation of wave activity from the troposphere between 20° and 40°S. Dividing the analysis up into two longitude regions, Pacific and Not Pacific, which have rather different tropospheric zonal wind responses, reveals that the enhanced upward flux of wave activity into the lower stratosphere consists of two distinct components. In Not Pacific, where there is an equatorward shift of the SH eddy-driven midlatitude jet, there is an enhanced flux of wave activity from high phase speed eddies ($c_A \sim$ 12–30 m s^{-1}) related to a change in the source of these eddies from the lower troposphere due to the shift in jet position. In Pacific, where there is a strengthened subtropical zonal wind but no equatorward shift of the midlatitude jet, there is an enhanced source of low phase speed eddies in the region between the subtropical and midlatitude jets. These seem likely to be related to the interjet disturbances found by Kim and Lee (2004) and

Lee (1997), although their exact nature is not yet well understood and requires further investigation.

The lack of a resolved wave drag anomaly in the NH can be understood from the projection of the zonal wind anomaly onto the climatology there. There are essentially no NH zonal wind anomalies in Not Pacific. In Pacific, unlike in the SH, the enhanced subtropical zonal wind does not increase the extent of the interjet region; rather, it enhances the barotropic shear on the equatorward side of the jet. The existence of different climatologies in the two hemispheres during this season means that a very similar subtropical wind anomaly has rather different effects. In particular, in the NH there is a reduced, rather than an enhanced, upward flux of low phase speed eddies. While there is an enhanced upward flux of the higher phase speed eddies associated with the strengthening and equatorward shifting of the NH midlatitude jet, the sum of the low and high phase speed

anomalies results in only a very small change in resolved wave drag.

This study has focused on the response in December–March. This is the season when the lower stratospheric response to ENSO is largest, both in observations and in our simulations. However, a smaller temperature response is also found in other seasons. Some preliminary analysis of these seasons suggests a decline in the anomaly until NH summer when the anomaly increases again. However, in this season the mechanism is likely to be different and seems to be predominantly associated with stationary waves in the NH subtropics.

The mechanisms behind the circulation changes have been proposed via a modeling study and it is important to ask whether they are supported by observations. Figure 3 of Free and Seidel (2009) shows that in December–February (DJF) the warming of the extratropical lower stratosphere in response to El Niño is stronger and more significant in the SH than the NH. This SH midlatitude warming can only be explained by a subtropical wave drag anomaly in the SH. Furthermore, the tropospheric zonal wind anomalies produced by CMAM are very similar to those found in observations (L'Heureux and Thompson 2006; Seager et al. 2003). In particular, there is an accelerated wind in the subtropics of both hemispheres that projects onto the climatology in the same way as in CMAM. Also, the equatorward shifting of the eddy-driven midlatitude jet at longitudes other than the Pacific region in the SH is evident in observations (Seager et al. 2003). Thus, the wind anomalies required to produce the eddy flux anomalies exist in the real atmosphere. Given that the ENSO forcing is of tropospheric origin, it is likely that the tropospheric zonal wind anomalies are primarily associated with the tropospheric response to that tropospheric forcing; then given those tropospheric zonal wind anomalies the stratospheric circulation changes can be explained via the proposed mechanisms.

There are at least two open questions that require further investigation. The first is the exact mechanism behind the tropospheric zonal wind response to ENSO. There have been advances (Robinson 2002; Seager et al. 2003; Lu et al. 2008; Harnik et al. 2010) but certain aspects of the response remain unclear, such as the origin of the zonal asymmetries in the midlatitude responses. The second is the exact nature of these lower phase speed disturbances and the factors that influence their generation.

REFERENCES

Andrews, D. G., J. R. Holton, and C. B. Leovy, 1987: *Middle Atmosphere Dynamics*. Academic Press, 489 pp.

Brönnimann, S., 2007: Impact of El Niño–Southern Oscillation on European climate. *Rev. Geophys., 45,* RG3003, doi:10.1029/2006RG000199.

Calvo, N., R. R. Garcia, W. J. Randel, and D. R. Marsh, 2010: Dynamical mechanism for the increase in tropical upwelling in the lowermost tropical stratosphere during warm ENSO events. *J. Atmos. Sci., 67,* 2331–2340.

Chiang, J. C. H., and A. H. Sobel, 2002: Tropical tropospheric temperature variations caused by ENSO and their influence on the remote tropical climate. *J. Climate, 15,* 2616–2631.

Deckert, R., and M. Dameris, 2008: Higher tropical SSTs strengthen the tropical upwelling via deep convection. *Geophys. Res. Lett., 35,* L10813, doi:10.1029/2008GL033719.

Dunkerton, T., C.-P. F. Hsu, and M. E. McIntyre, 1981: Some Eulerian and Lagrangian diagnostics for a model stratospheric warming. *J. Atmos. Sci., 38,* 819–843.

Eyring, V., T. G. Shepherd, and D. W. Waugh, Eds., 2010: SPARC report on the evaluation of chemistry–climate models. SPARC Rep. 5, WCRP–132, WMO/TD 1526. [Available online at http://www.atmosp.physics.utoronto.ca/SPARC/ccmval_final/index.php.]

Free, M., and D. J. Seidel, 2009: Observed El Niño–Southern Oscillation temperature signal in the stratosphere. *J. Geophys. Res., 114,* D23108, doi:10.1029/2009JD012420.

Garcia-Herrera, R., N. Calvo, R. R. Garcia, and M. A. Giorgetta, 2006: Propagation of ENSO temperature signals into the middle atmosphere: A comparison of two general circulation models and ERA-40 reanalysis data. *J. Geophys. Res., 111,* D06101, doi:10.1029/2005JD006061.

Hardiman, S. C., N. Butchart, P. H. Haynes, and S. H. E. Hare, 2007: A note on forced versus internal variability of the stratosphere. *Geophys. Res. Lett., 34,* L12803, doi:10.1029/2007GL029726.

Harnik, N., R. Seager, N. Naik, M. Cane, and M. Ting, 2010: The role of linear wave refraction in the transient eddy–mean flow response to tropical Pacific SST anomalies. *Quart. J. Roy. Meteor. Soc., 136,* 2132–2146.

Hayashi, Y., 1971: A generalized method of resolving disturbances into progressive and retroprogressive waves by space Fourier and time cross-spectral analyses. *J. Meteor. Soc. Japan, 49,* 125–128.

Haynes, P. H., C. J. Marks, M. E. McIntyre, T. G. Shepherd, and K. P. Shine, 1991: On the "downward control" of extratropical diabatic circulations by eddy-induced mean zonal forces. *J. Atmos. Sci., 48,* 651–678.

Holton, J. R., 1990: On the global exchange of mass between the stratosphere and troposphere. *J. Atmos. Sci., 47,* 392–395.

Hoskins, B. J., and D. J. Karoly, 1981: The steady linear response of a spherical atmosphere to thermal and orographic forcing. *J. Atmos. Sci., 38,* 1179–1196.

James, I. N., 1987: Suppression of baroclinic instability in horizontally sheared flows. *J. Atmos. Sci.,* **44,** 3710–3720.

——, and L. J. Gray, 1986: Concerning the effect of surface drag on the circulation of a baroclinic planetary atmosphere. *Quart. J. Roy. Meteor. Soc.,* **112,** 1231–1250.

Kim, H., and S. Lee, 2004: The wave–zonal mean flow interaction in the Southern Hemisphere. *J. Atmos. Sci.,* **61,** 1055–1067.

Lee, S., 1997: Maintenance of multiple jets in a baroclinic flow. *J. Atmos. Sci.,* **54,** 1726–1738.

L'Heureux, L. M., and D. W. J. Thompson, 2006: Observed relationships between the El Niño–Southern Oscillation and the extratropical zonal-mean circulation. *J. Climate,* **19,** 276–287.

Li, F., J. Austin, and J. Wilson, 2008: The strength of the Brewer–Dobson circulation in a changing climate: Coupled chemistry–climate model simulations. *J. Climate,* **21,** 40–57.

Lu, J., G. Chen, and D. M. W. Frierson, 2008: Response of the zonal mean atmospheric circulation to El Niño versus global warming. *J. Climate,* **21,** 5835–5851.

Manzini, E., M. A. Giorgetta, M. Esch, L. Kornblueh, and E. Roeckner, 2006: The influence of sea surface temperatures on the northern winter stratosphere: Ensemble simulations with the MAECHAM5 model. *J. Climate,* **19,** 3863–3881.

Marsh, D. R., and R. R. Garcia, 2007: Attribution of decadal variability in lower-stratospheric tropical ozone. *Geophys. Res. Lett.,* **34,** L21807, doi:10.1029/2007GL030935.

McLandress, C., and T. G. Shepherd, 2009: Simulated anthropogenic changes in the Brewer–Dobson circulation, including its extension to high latitudes. *J. Climate,* **22,** 1516–1540.

Morgenstern, O., and Coauthors, 2010: Review of the formulation of present-generation stratospheric chemistry-climate models and associated external forcings. *J. Geophys. Res.,* **115,** D00M02, doi:10.1029/2009JD013728.

Randel, W. J., and I. M. Held, 1991: Phase speed spectra of transient eddy fluxes and critical layer absorption. *J. Atmos. Sci.,* **48,** 688–697.

——, and A. M. Thompson, 2011: Interannual variability and trends in tropical ozone derived from SAGE II satellite data and SHADOZ ozonesondes. *J. Geophys. Res.,* **116,** D07303, doi:10.1029/2010JD015195.

——, R. R. Garcia, N. Calvo, and D. Marsh, 2009: ENSO influence on zonal mean temperature and ozone in the tropical lower stratosphere. *Geophys. Res. Lett.,* **36,** L15822, doi:10.1029/2009GL039343.

Rayner, N. A., D. E. Parker, E. B. Horton, C. K. Folland, L. V. Alexander, D. P. Rowell, E. C. Kent, and A. Kaplan, 2003: Global analyses of sea surface temperature, sea ice, and night marine air temperature since the late nineteenth century. *J. Geophys. Res.,* **108,** 4407, doi:10.1029/2002JD002670.

Reid, G. C., K. S. Gage, and J. R. McAfee, 1989: The thermal response of the tropical atmosphere to variations in equatorial Pacific sea surface temperature. *J. Geophys. Res.,* **94,** 14 705–14 716.

Robinson, W. A., 2002: On the midlatitude thermal response to tropical warmth. *Geophys. Res. Lett.,* **29,** 1190, doi:10.1029/2001GL014158.

Sassi, F., D. Kinnison, B. A. Boville, R. R. Garcia, and R. Roble, 2004: Effect of El Niño–Southern Oscillation on the dynamical, thermal, and chemical structure of the middle atmosphere. *J. Geophys. Res.,* **109,** D17108, doi:10.1029/2003JD004434.

Sato, M., J. E. Hansen, M. P. McCormick, and J. B. Pollack, 1993: Stratospheric aerosol optical depths, 1850–1990. *J. Geophys. Res.,* **98,** 22 987–22 994.

Scinocca, J. F., N. A. McFarlane, M. Lazare, J. Li, and D. Plummer, 2008: The CCCma third generation AGCM and its extension into the middle atmosphere. *Atmos. Chem. Phys.,* **8,** 7055–7074.

Seager, R., N. Harnick, Y. Kushnir, W. Robinson, and J. Miller, 2003: Mechanisms of hemispherically symmetric climate variability. *J. Climate,* **16,** 2960–2978.

Shepherd, T. G., and C. McLandress, 2011: A robust mechanism for strengthening of the Brewer–Dobson circulation under climate change: Critical-layer control of subtropical wave breaking. *J. Atmos. Sci.,* **68,** 784–797.

Taguchi, M., and D. L. Hartmann, 2006: Increased occurrence of stratospheric sudden warmings during El Niño as simulated by WACCM. *J. Climate,* **19,** 324–332.

Trenberth, K. E., 1997: The definition of El Niño. *Bull. Amer. Meteor. Soc.,* **78,** 2771–2777.

Yulaeva, E., and J. M. Wallace, 1994: The signature of ENSO in global temperature and precipitation fields derived from the Microwave Sounding Unit. *J. Climate,* **7,** 1719–1736.